Hydrol. Earth Syst. Sci. Discuss., 9, 5167–5193, 2012
www.hydrol-earth-syst-sci-discuss.net/9/5167/2012/
doi:10.5194/hessd-9-5167-2012

Hydrology and Earth System Sciences Discussions

On the utility of land surface models for agricultural drought monitoring

W. T. Crow[1], S. V. Kumar[2,3], and J. D. Bolten[2]

[1]USDA Hydrology and Remote Sensing Laboratory, Beltsville, MD, USA
[2]NASA Goddard Space Flight Center, Greenbelt, MD, USA
[3]Science Applications International Corporation, Beltsville, MD, USA

Received: 16 March 2012 – Accepted: 5 April 2012 – Published: 19 April 2012

Correspondence to: W. T. Crow (wade.crow@ars.usda,gov)

Published by Copernicus Publications on behalf of the European Geosciences Union.

Abstract

The lagged rank cross-correlation between model-derived root-zone soil moisture estimates and remotely-sensed vegetation indices (VI) is examined between January 2000 and December 2010 to quantify the skill of various soil moisture models for agricultural drought monitoring. Examined modeling strategies range from a simple antecedent precipitation index to the application of modern land surface models (LSMs) based on complex water and energy balance formations. A quasi-global evaluation of lagged VI/soil moisture cross-correlation suggests, when averaged in bulk across the annual cycle, little or no added skill (<5 % in relative terms) is associated with applying modern LSMs to off-line agricultural drought monitoring relative to simple accounting procedures based solely on observed precipitation accumulations. However, slightly larger amounts of added skill (5–15 % in relative terms) are identified when focusing exclusively on the extra-tropical growing season and/or utilizing soil moisture values acquired by averaging across a multi-model ensemble.

1 Introduction

Agricultural drought is commonly defined as the lack of sufficient soil water availability to maintain adequate crop growth and pasture productivity (Panu and Sharma, 2002). The development of large-scale drought agricultural monitoring systems has received considerable attention in the past decade, and a range of remote sensing, ground observation, and land surface modeling techniques have been proposed in an effort to improve the early detection of agricultural drought and the efficiency of subsequent mitigation responses (Wardlow et al., 2012). One common approach has been the application of complex water balance formulations embedded within land surface models (LSMs) to track temporal anomalies in root-zone soil water availability (Mo et al., 2010; Sheffield et al., 2012). These models typically include water and energy balance formulations based on time-varying meteorological and radiative forcing as well as detailed

HESSD
9, 5167–5193, 2012

Drought monitoring utility

W. T. Crow et al.

vertical soil physics to describe sub-surface soil water soil flux and storage. As a result, these "modern" LSMs implicitly promise an enhanced representation of root-zone soil water dynamics relative to soil moisture proxy products based solely on the simple accounting of antecedent precipitation. Recent work has also focused on the potential for improving soil moisture predictions by averaging across a multi-model ensemble comprised of various LSMs (Guo et al., 2007). Despite this potential, quantifying the marginal value of modern LSMs for global drought monitoring is challenging due to a lack of adequate large-scale root-zone soil water datasets available for evaluation purposes (Bolten et al., 2010).

Recently, Peled et al. (2010) proposed a novel approach for evaluating LSM soil moisture predictions by examining the cross-correlation between model-estimated root-zone soil moisture anomalies and spatially concurrent anomalies in vegetation indices derived from visible/near-infrared (VIS/NIR) remote sensing. The use of VIS/NIR vegetation indices (VI) like the Enhanced Vegetation Index (EVI) and the Normalized Difference Vegetation Index (NDVI) is well-established for monitoring the extent and severity of agricultural drought (Kogan, 1995; Peters et al., 2002; Ji and Peters, 2003). The potential of root-zone soil moisture monitoring lies in its ability to provide a leading indicator of subsequent VI anomalies (Adegoke and Carleton, 2002; Ji and Peters, 2005; Musyimi, 2010). That is, under water-limited conditions, a negative soil moisture anomaly should temporally precede a detectable impact on vegetation health and biomass. The analysis in Peled et al. (2010) is based on the assumption that the strength of lagged soil moisture/VI cross-correlation can be used as a large-scale proxy for the accuracy of a model-based, root-zone soil moisture product.

Here we expand the geographic scope of Peled et al. (2010) (from the European continent to all global land between 60° S and 60° N) and evaluate a wider range of potential land surface modeling strategies. In particular, this analysis will employ various global LSMs, ranging from complex, modern LSMs to a simple antecedent precipitation index to sample lagged rank-correlations between model-estimated soil moisture and remotely-sensed VI products. These cross-correlations will then be examined for

Discussion Paper | Discussion Paper | Discussion Paper | Discussion Paper |

HESSD

9, 5167–5193, 2012

Drought monitoring utility

W. T. Crow et al.

evidence that higher-order water and energy processes captured by modern LSMs, but neglected in simple accounting procedures based solely on antecedent precipitation, add significant marginal utility to agricultural drought monitoring. In addition to evaluating stand-alone LSM predictions, the advantages of acquiring soil moisture products from a multi-model ensemble will also be quantified.

2 Models and data

The analysis is based on root-zone soil moisture products extracted from four separate models: version 3.2 of the National Centers for Environmental Prediction, Oregon State University, Air Force Weather Office and National Weather Service Hydrologic Research Laboratory model (Noah) (Ek et al., 2003; Mitchell, 2005; Barlarge et al., 2010), version 2.0 of the Common Land Model (CLM) (Dai et al., 2003), the Catchment Land Surface Model (CLSM) (Koster et al., 2000; Ducharne et al., 2000) and, as an obviously simplified baseline approach, an antecedent precipitation index (API). All models are run on a global 0.25° grid between 1 January 2000 and 31 December 2010 for all global land areas between 60° S and 60° N. Noah, CLM, and CLSM are run on a half-hourly time step while API calculations are based on a daily time step. For each model, a 1 January 2000 initialization is derived by separately looping each model through three integrations of this time period.

2.1 Soil moisture models

Noah, CLM, and CLSM simulations are conducted using the NASA Land Information System (LIS) data assimilation test-bed which provides a framework for the integrated use of several community LSMs (Kumar et al., 2006). All three models dynamically predict vertically-discretized profile soil moisture based on a complex vertical representation of water flow within the soil column and surface energy balance approaches for the estimation of evapotranspiration. In addition to precipitation, modern LSMs require

HESSD
9, 5167–5193, 2012

air temperature, air pressure, relatively humidity, wind speed, and radiation (both short-wave and long-wave) forcing data as input. Vertical soil water processes (e.g., infiltration and drainage) vary as a function of soil hydraulic properties typically tied to soil textural classifications through pedo-transfer functions. Energy balance processes depend strongly on land surface parameters like albedo, surface roughness, and leaf area index parameters typically specified as a function of vegetation class or climatological VI information. While the focus here is on the growing season, it should be noted that Noah, CLM, and CLSM all contain snow modules which account for the accumulation, retention and melting of snow water storage.

Root-zone soil moisture is nominally defined as LSM-predicted soil moisture for the top 1-meter of the soil column (θ). For this particular implementation, Noah uses four soil layers with thicknesses of 10, 30, 60, and 100 cm (descending from the surface), and CLM uses ten soil layers with thicknesses of 1.75, 2.76, 4.55, 7.5, 12.36, 20.38, 33.60, 55.39, 91.33, and 113.7 cm. Consequently, the top three Noah layers and top eight CLM layers are averaged (using relative weights equal to the ratio of each layer thickness to the 1-m total root-zone depth) to obtain an integrated root-zone soil moisture product. The Catchment LSM, by contrast, is non-traditional in that the vertical soil moisture profile is determined through deviations from the equilibrium soil moisture profile between the surface and the water table. In the CLSM, soil moisture is calculated within a 2-cm surface layer and a 1-m root-zone layer is diagnosed from the modeled soil moisture profile (Koster et al., 2000). All three modern LSMs (Noah, CLM, and CLSM) are run on a half-hourly time step continuously throughout the year.

An API-based root-zone soil water proxy (θ_{API}) is calculated as a linear combination of the previous day's value ($\theta_{\mathrm{API},j-1}$) and accumulated precipitation (in mm) for the current day (P_j):

$$\theta_{\mathrm{API},j} = \gamma\,\theta_{\mathrm{API},j-1} + P_j \tag{1}$$

where the constant parameter γ controls the effective memory of API levels to past rainfall accumulations. Unlike the modern LSMs described above, the API model explicitly

HESSD
9, 5167–5193, 2012

ignores variations in root-zone soil moisture storage due to surface energy balance processes (e.g., evapotranspiration and/or net radiation), the vertical and/or lateral movement of water between multiple soil moisture states, and the impact of snow melt on soil water availability.

2.2 Forcing and evaluation data

All three modern LSMs (i.e., Noah, CLM, and CLSM) are driven by two separate forcing data sets which provide fine-scale (hourly to three-hourly) values of: precipitation, insolation, air temperature, humidity, wind speed, and air pressure. The first data set is derived from the Global Data Assimilation System (GDAS) obtained from the weather forecast model of the National Centers for Environmental Prediction (Derber et al., 1991). In order to mitigate known biases in GDAS precipitation fields, coarse-resolution rainfall accumulations are based on the NOAA Climate Prediction Center's (CPC) operational global 2.5°, 5-day Merged Analysis of Precipitation (CMAP) product (Xie and Arkin, 1997) which blends satellite and rain-gauge observations. The GDAS modeled precipitation fields are then used only to temporally and spatially disaggregate CMAP accumulation totals.

While this "GDAS+CMAP" product is representative of currently-available global LSM forcing datasets, higher-quality forcing data sets are available in selected continental areas. To reflect this, the modern LSMs are also forced with the North American Land Data Assimilation System Version 2 (NLDAS-2) forcing dataset (Xia et al., 2012) within a regional domain centered on the contiguous United States (CONUS) (25.75°–52° N, 124°–68.75° W). Relative to GDAS+CMAP, the NLDAS-2 dataset is based on regional (as opposed to global) reanalysis products and leverages a greater abundance of ground and satellite-based observational resources. In particular, NLDAS-2 precipitation is based on the merger of: daily CPC rain gauge accumulations with ground-based radar, satellite-based precipitation, and North American Regional Reanalysis (NARR) precipitation fields (Cosgrove et al., 2003). Incoming long-wave and shortwave radiation estimates are taken from the NASA/GEWEX Surface Radiation

Budget (SRB) dataset and geostationary satellite observations. Remaining NLDAS-2 forcing variables (e.g., air temperature, wind speed, relative humidity, and air pressure) are based on NCEP North American Regional Reanalysis (NARR).

Modern LSMs generally input remotely-sensed VI information to estimate vegetation parameters. Here, all such parameters are derived from climatological VI information derived from long-term Advanced Very High Resolution Radiometer (AVHRR) surface reflectance products. Since they lack inter-annual variability, the use of climatological VI information as LSM input minimizes the risk of error cross-correlation between LSM soil moisture predictions and annual variations in VI used for evaluation purposes. Additional land cover information is derived from the 1-km University of Maryland land cover classification (Hansen et al., 2000). Assumed soil texture is obtained by merging the global Foreign Agricultural Office (FAO) soil classification product with the State Soil Geographic (STATSGO) database within CONUS.

In contrast, the API model is forced solely by daily (00:00 to 24:00 UTC) precipitation accumulations acquired by temporally aggregating sub-daily GDAS+CMAP and/or NLDAS-2 precipitation accumulations. The single parameter γ is assumed to be a fixed global constant (see below). NDVI values used for evaluation purposes are taken from the monthly Moderate Resolution Imaging Spectroradiometer (MODIS) MOD13C2 composite product (Collection 5) between February 2000 and December 2010. Only reliable MODIS VI retrievals categorized as “Good data – use with confidence” in the MOD13C2 pixel reliability field are included in the analysis and spatially aggregated to match the 0.25° LSM modeling grid.

3 Analysis

The analysis is based on the assumption that higher-quality root-zone soil moisture data sets will exhibit stronger lagged correlations with future VI anomalies (Peled et al., 2010). However, secondary characteristics like climatological seasonality, distribution shape, and temporal auto-correlation can also impact soil moisture/VI cross-correlations.

HESSD
9, 5167–5193, 2012

In order to minimize these effects, results are based on rank correlations sampled after the transformation of both raw VI and soil moisture data into a monthly rank time series and the standardization of soil moisture auto-correlation functions. See below for a description of this processing.

3.1 Rank time series calculation

To begin, every model-based root-zone soil moisture product θ is aggregated to create a monthly time series $\bar{\theta}_i$ from January 2000 to December 2010 for each 0.25° land pixel between 60° S and 60° N. Next, $\bar{\theta}_i$ for a single month i (and single 0.25° land pixel) are ranked across all eleven occurrences of the same month-of-year between 2000 and 2010 for the same pixel. As a result, the $\bar{\theta}$ time series is transformed into a monthly time series of ranks – or $\mathrm{Rank}(\bar{\theta})_i$ – which reflect the relative wetness of a particular month relative to the same month during all other years. The same ranking procedure is applied to monthly NDVI to create $\mathrm{Rank}(\overline{\mathrm{NDVI}})_i$. This rank transformation accomplishes two key things. First, it removes the seasonal cycle from each product so that the analysis focuses solely on inter-annual variations. Second, it ensures a consistent distribution for variables in the cross-correlation analysis and minimizes the potential impact of outliers. The use of a monthly time scale is intended as a compromise between minimizing the temporal resolution of the analysis while maximizing the spatial coverage and completeness of composited VI products.

Figure 1 shows example times series of monthly $\mathrm{Rank}(\bar{\theta}_{\mathrm{Noah}})$ and $\mathrm{Rank}(\overline{\mathrm{NDVI}})$ for a single 0.25° pixel in the Southern Great Plains of the United States. Formally, the y-axis describes the fractional rank of month i relative to the same month-of-year found in other years of the 2000 to 2010 time period (i.e., the fraction of the same month-of-year in different years with lower $\bar{\theta}$ or lower $\overline{\mathrm{NDVI}}$). Periodic gaps in the NDVI time series reflect months where MODIS-based NDVI products are deemed unreliable.

Discussion Paper | Discussion Paper | Discussion Paper | Discussion Paper |

HESSD

9, 5167–5193, 2012

Drought monitoring utility

W. T. Crow et al.

3.2 Rank auto-correlation analysis and standardization

Despite the fact that Noah, CLM, and CLSM root-zone products are all defined to provide top-1-m soil moisture products, differences in evapotranspiration and drainage parameterizations between models can induce variations in the effective persistence of soil moisture anomalies. Such differences can, in turn, impact sampled soil moisture/VI cross-correlation. To address this, the auto-correlation function of $\text{Rank}(\bar{\theta})_i$ – or $\rho(L)$ – is standardized across all models prior to further cross-correlation analysis. With this goal in mind, Fig. 2a plots quasi-global averages (i.e., land areas between 60° S and 60° N) of $\rho(L)$ for root-zone soil moisture estimates from Noah, CLM, and CLSM. For top-1-meter LSM results, CLM, and CLSM $\rho(L)$ results match relatively closely. However, 1-m Noah results show significantly more temporal auto-correlation. Consequently, all subsequent Noah results are instead based on a shallower vertical integration of soil moisture (i.e., top 40-cm versus top-1-m). Unlike the original 1-m results, 40-cm Noah soil moisture results provide a close match to 1-m CLM and CLSM $\rho(L)$ results. Also note that the resulting $\rho(L)$ functions show considerable temporal auto-correlation at lags of ±1-month – suggesting that a monthly time scale represents a reasonable temporal support for capturing root-zone soil moisture dynamics.

API results are based on calibrating γ in (1) to produce quasi-globally-averaged API-based $\rho(L)$ results which approximate that of the modern LSMs. However, due to differences in the in the shape of API's $\rho(L)$ function relative to the modern LSMs there is some ambiguity in this calibration. Figure 2b illustrates this effect by comparing quasi-globally-averaged $\rho(L)$ for $\gamma = 0.98$, 0.985, and 0.99 to the absolute range of $\rho(L)$ results for Noah, CLM, and CLSM. Note that $\gamma = 0.98$ represents a plausible fit to the modern LSM range for $|L| = 1$ but drifts badly for larger $|L|$. Conversely, $\gamma = 0.99$ is adequate at large $|L|$ but poor for small $|L|$. While the middle choice of $\gamma = 0.985$ minimizes misfits over the entire range of L, it still performs badly at large $|L|$. Unless otherwise noted, all future API results will be for the middle case $\gamma = 0.985$. However,

HESSD
9, 5167–5193, 2012

given the ambiguity noted in Fig. 2b, the sensitivity of key API results to γ will also be noted.

3.3 Ensemble-mean product

As described above, a final soil moisture product is created by averaging across soil moisture results within a multi-model ensemble. This product is based on transforming each of the four monthly root-zone soil moisture products ($\bar{\theta}_{\text{Noah}}$, $\bar{\theta}_{\text{CLM}}$, $\bar{\theta}_{\text{CLSM}}$ and $\bar{\theta}_{\text{API}}$) into their standard normal deviates:

$$\bar{\theta}'_i = \frac{\bar{\theta}_i - \mu_{\bar{\theta}}}{\sigma_{\bar{\theta}}} \tag{2}$$

where $\mu_{\bar{\theta}}$ and $\sigma_{\bar{\theta}}$ are the sampled mean and standard-deviation, respectively, for each $\bar{\theta}$ product during all occurrences of the month-of-year associated with month i. Next, all four anomaly products are averaged to create a monthly ensemble-averaged product:

$$\bar{\theta}'_{\text{ENS},i} = \frac{1}{4}\left(\bar{\theta}'_{\text{Noah},i} + \bar{\theta}'_{\text{CLM},i} + \bar{\theta}'_{\text{CLSM},i} + \bar{\theta}'_{\text{API},i}\right). \tag{3}$$

The resulting time-series of $\bar{\theta}'_{\text{ENS}}$ are then ranked to create $\text{Rank}(\bar{\theta}_{\text{ENS}})$. Note that the anomaly notation is dropped when referring to this rank product since $\text{Rank}(\bar{\theta}_{\text{ENS}}) = \text{Rank}(\bar{\theta}'_{\text{ENS}})$.

3.4 Rank cross-correlation calculation

The Spearman rank cross-correlation $R(L)$ at lag L between NDVI and all five root-zone soil moisture rank products (i.e., $\text{Rank}(\bar{\theta}_{\text{Noah}})$, $\text{Rank}(\bar{\theta}_{\text{CLM}})$, $\text{Rank}(\bar{\theta}_{\text{CLSM}})$, $\text{Rank}(\bar{\theta}_{\text{ENS}})$, and $\text{Rank}(\bar{\theta}_{\text{API}})$) is calculated as the sampled correlation coefficient between $\text{Rank}(\bar{\theta})_{i+L}$ and $\text{Rank}(\overline{\text{NDVI}})_i$ over all possible i. Based on this definition, $R(L)$ for $L < 0$ relates the ability of *current* soil moisture conditions to forecast *future* NDVI. It is important to

HESSD
9, 5167–5193, 2012

note that positive $R(L)$ is not be expected for all biomes or land cover types. For example, in energy-limited areas, relatively dry periods may be associated with enhanced VI due to reduced cloudiness (Huete et al., 2006). In these areas, an increase in $R(L)$ (i.e., making it less negative) cannot be reliability linked to improved soil moisture skill. Therefore, all 0.25° pixels in which the null hypothesis $R(-1) >= 0$ can be rejected (at 80 % significance) for *any* model product is subsequently masked from the entire analysis. In order to minimize the impact of cold-season conditions, months with an average daily high air temperature below 5 °C are also removed (on a month-by-month and pixel-by-pixel basis).

4 Results

For the case $L = -1$ (i.e., $\text{Rank}(\bar{\theta})$ temporally precedes $\text{Rank}(\overline{\text{NDVI}})$ by 1 month), Fig. 3 plots global, 0.25° Noah, CLM, CLSM, ENS and API $R(-1)$ results. White masked areas represent a combination of open water surfaces, areas with non-significant positive $R(-1)$ (see above), and barren areas where no temporal NDVI variability is observed. Substantial coupling ($R(-1) > 0.50$) is found in semi-arid areas of the world prone to water-limited plant growth (e.g., Australia, Southern Africa, and the Western United States). Conversely, humid areas of the Eastern United States, Europe, and Southeastern Asia demonstrate weak soil moisture/VI cross-correlation ($R(-1) < 0.20$). A secondary cause of low $R(-1)$ is poor accuracy in model-based soil moisture predictions. For example, low sampled $R(-1)$ in arid regions of sub-Saharan Africa are likely caused by inadequate rain gauge coverage which prevents LSMs from accurately capturing relative soil moisture variations in data-poor regions.

Figure 4 examines model-to-model differences in performance between models by plotting spatially-distributed Z-scores for sampled $R(-1)$ differences between the four approaches based on modern LSM simulations (i.e., Noah, CLSM, CLM, and ENS) and the API baseline. Since the Fischer transformation

$$F(R) = \frac{1}{2}\,\mathrm{Ln}([1+R]/[1-R]) \tag{4}$$

of sampled R yields a normal distribution with variance $1/(n-1)$ (Van Storch and Zwiers, 2004), Z-scores for $R(-1)$ differences between an LSM and API can be calculated as:

$$Z = \sqrt{\frac{n-1}{2}}\left(F[R_{\mathrm{LSM}}(-1)] - F[R_{\mathrm{API}}(-1)]\right) \tag{5}$$

where n is taken to be the number of months sampled to obtain $R(-1)$. Note that since Eq. (5) neglects the impact of temporal auto-correlation in both $\mathrm{Rank}(\overline{\mathrm{NDVI}})$ and $\mathrm{Rank}(\bar{\theta})$, these Z-scores are likely not appropriate for formal hypothesis testing. Nevertheless, they represent a useful tool for standardizing observed model-to-model differences. While regions of significantly improved NDVI forecasting (relative to API) exist in Noah, CLM, and CLSM predictions (i.e., positive Z scores indicated by red shading in Fig. 4), they are balanced by areas where API-based soil moisture products are superior (i.e., negative Z-scores indicated by blue shading in Fig. 4). Only the multi-model ENS case appears to consistently improve upon the API baseline.

Figure 5a compares modeling results on a quasi-global scale by plotting average $R(L)$ across all unmasked land areas in Fig. 3 for a range of L. Sampled $R(L)$ functions are not symmetric with respect to $L = 0$, and instead are larger for $L < 0$. This lack of symmetry underscores the predictive role for soil moisture where the largest $R(L)$ is sampled for the $L < 0$ case where $\mathrm{Rank}(\bar{\theta})$ precedes $\mathrm{Rank}(\overline{\mathrm{NDVI}})$. Using Eqs. (4) and (5), error bars can be constructed for individual points in Fig. 5. However, even if conservative reductions in effective degrees of freedom are made to account for potential spatial and temporal autocorrelation in $\mathrm{Rank}(\overline{\mathrm{NDVI}})$ and $\mathrm{Rank}(\bar{\theta})$, 1σ sampling uncertainty associated with these quasi-global averages of $R(-1)$ remains on the order of 0.005 [-] to 0.001 [-] and therefore smaller than the size of plotted symbols in

Fig. 5. Consequently, it is safe to assume that all visible differences in plotted $R(L)$ are significant at a 1σ certainty level.

Nevertheless, among the stand-alone models, the relative magnitude of model-to-model variations is small. For $L < 0$, Noah, CLM, and CLSM results are associated with $R(L)$ values that fall within about ±5 % of baseline API results (Fig. 5b). That is, none of the stand-alone modern LSMs demonstrate any substantial advantage over API in anticipating the near-term impact of agricultural drought on NDVI anomalies. However, using a multi-model ensemble average acquired from Eq. (3) leads to a larger (and more consistent) amount of improvement relative to the API baseline (see Fig. 5b). As a result, the only viable method for increasing $R(L)$ through the use of modified model physics appears to lie in the use of multi-model ensembles.

Utilizing EVI as the target VI (not shown) produces a qualitatively similar plot except sampled $R(L)$ values are somewhat lower than those found using NDVI for all modeling cases. Likewise, API $R(L)$ results in Fig. 5 are slightly improved when using lower values of γ in Eq. (1); however, the overall effect is very small. For example, reducing γ from 0.99 to 0.98 (i.e., covering the entire plausible range of γ indentified in Fig. 2b) increases globally-average API $R(-1)$ results by only ~2 % (not shown).

4.1 Impact of forcing data quality

Since modern LSMs attempt to exploit temporal variations in non-rainfall based forcing (e.g., air temperature and insolation) to better predict soil moisture anomalies, one factor impacting the performance spread between modern LSMs and an API baseline may be the quality of non-rainfall forcing data. Figure 6 looks at the impact of replacing the global GDAS + CMAP forcing dataset with the higher-quality (but non-global) NLDAS-2 dataset. Dashed lines in Fig. 6a show CONUS GDAS + CMAP $R(L)$ results for each model and solid lines NLDAS-2 results for the same CONUS domain. For clarity, ENS results are omitted. The transition between GDAS+CMAP and NLDAS-2 forcing clearly improves the performance of the models. However, nearly all of this improvement is attributable to improved rainfall since there is no discernible improvement in modern LSM

HESSD
9, 5167–5193, 2012

results relative to API (Fig. 6b). In fact, for $L < -4$, utilizing NLDAS-2 forcing actually degrades the quality of the modern LSM forcings relative to API (Fig. 6b). Consequently, there is no evidence that enhancing the quality of non-rainfall forcing data improves the performance of modern LSMs relative to the API baseline.

4.2 Impact of seasonality

Large seasonal variability in soil water availability, and thus $R(L)$, is expected in certain climate zones. To examine such seasonal variability, Fig. 7 plots spatially-averaged $R(-1)$ within various latitude bands according to the month-of-year for $\mathrm{Rank}(\bar{\theta})$ obtained using GDAS+CMAP forcings. In order to ensure the consistent spatial support of sampled $R(-1)$ among different months, the monthly air temperature mask (see Sect. 3) is not applied here. Observed monthly trends in Fig. 7 conform well to expected seasonal patterns. For instance, in the extra-tropical Northern Hemisphere (ETNH; Fig. 7a) the highest soil moisture/vegetation coupling, and thus sampled $R(-1)$, occurs during the boreal summer when root-zone soil moisture is generally minimized. Likewise, seasonal $R(-1)$ trends in tropical regions (Figs. 7b and c) reflect the expected progression of the tropical rain belt with relatively lower $R(-1)$ found during the rainy seasons for both the tropical Northern Hemisphere (TNH; May to October) and tropical Southern Hemisphere (TSH; November to April).

Figure 8 mirrors Fig. 5a by plotting results in Fig. 7 in terms of percentage variation versus an API baseline. Despite relatively modest model-to-model variability in Fig. 7, several trends can be noted. For example, $R(-1)$ for Noah and CLM consistently improves upon the API baseline during mid-to-late portions of the ETNH growing season (see June to November results in Fig. 8a). The enhanced importance of evapotranspiration (on the overall soil water balance) in this period may increase the value of energy balance calculations made by modern LSMs. Likewise, during the end of both the TNH rainy season (September to November in Fig. 8b) and TSH rainy season (January to March in Fig. 8c), all three modern LSMs maintain a clear advantage over API.

HESSD
9, 5167–5193, 2012

5 Conclusions

Given the wide variety of remote sensing, ground observation, and modeling strategies currently being proposed for global agricultural drought monitoring (Wardlow et al., 2012), it is important to define benchmarking strategies capable of objectively evaluating the relative merits of each. Here, we quantify the added benefit of modern LSMs for anticipating future vegetation health and biomass anomalies relative to a baseline case of utilizing a much simpler antecedent precipitation index (API). Unlike API, modern LSMs offer a complex parameterization of the surface energy balance and detailed vertical water balance physics in an attempt to more accurately characterize temporal variations in root-zone soil moisture availability. However, when objectively evaluated at global scales over the entire seasonal cycle, modern LSMs offer little or no advantage versus an API baseline in terms of anticipating the impact of agricultural drought on vegetation condition (Figs. 3, 4, and 5). The relative utility of modern LSMs versus API is not enhanced by improving the quality of LSM forcing data (Fig. 6). Taken as a whole, results suggest that non-rainfall forcing data and modern LSM energy balance calculations contribute relatively little towards the accuracy of agricultural drought monitoring systems. As such, results are broadly consistent with past work in Abramowitz et al. (2008) questioning the general utility of LSM energy balance calculations, and imply that increasing LSM complexity is generally not an effective strategy for enhanced agricultural drought monitoring.

However, several caveats should be attached to this conclusion. Clear additive value does emerge when root-zone soil moisture estimates obtained from various models (including multiple modern LSMs) are merged into a single ensemble-mean prediction (Figs. 3 and 5). In addition, more added value (around 5 % to 15 % in relative terms) for modern LSMs is found during specific points along the seasonal cycle (Fig. 8) – particularly during middle to late portions of the ETNH growing season (see July to October in Fig. 8a). Given the importance of this period for agricultural drought monitoring, LSM performance during these months should (arguably) be given enhanced emphasis

HESSD
9, 5167–5193, 2012

when making overall assessments. Likewise, all results are based solely on the off-line application of LSMs and do not reflect the potential benefits of using a modern LSM in a coupled land/atmosphere modeling system. Such coupling could conceivably add skill to long-term precipitation forecasts and may therefore contribute to agricultural drought forecasting. Finally, even if their contribution to off-line drought prediction is marginal, modern LSMs may still have substantial utility in describing the subsequent impact of drought conditions on water balance processes like ET and runoff. Such diagnostic value cannot, of course, be duplicated by the API.

Acknowledgements. Research was supported by NASA Applied Sciences Grant entitled "Enhancing the USDA Global Crop Production Decision Support System with the NASA Land Information System and Water Cycle Satellite Observations" (W. T. Crow – Principal Investigator). Computing was partially supported by the resources at the NASA Center for Climate Simulation.

References

Abramowitz, G., Leuning, R., Clark, M., and Pitman, A.: Evaluating the performance of land surface models, J. Climate, 21, 5468–5481, 2008. 5181

Adegoke, J. O. and Carleton, A. M.: Relations between soil moisture and satellite vegetation indices in the US Corn Belt, J. Hydrometeorol., 3, 395–405, 2002. 5169

Barlage, M., Chen, F., Tewari, M., Ikeda, K., Gochis, D., Dudhia, J., Rasmussen, R., Livneh, B., Ek, M., and Mitchell, K.: Noah land surface model modifications to improve snowpack prediction in the colorado rocky mountains, J. Geophys. Res., 115, D22101, doi:10.1029/2009JD013470, 2010. 5170

Bolten, J. D., Crow, W. T., Jackson, T. J., Zhan, X., and Reynolds, C. A.: Evaluating the utility of remotely-sensed soil moisture retrievals for operational agricultural drought monitoring, IEEE J. Sel. Top. Appl., 3, 57–77, doi:10.1109/JSTARS.2009.2037163, 2010. 5169

Cosgrove, B. A., Lohmann, D., Mitchell, K. E., Houser, P. R., Wood, E. F., Schaake, J., Robock, A., Marshall, C., Sheffield, J., Luo, L., Duan, Q., Pinker, R. T., Tarpley, J. D., Higgins, R. W., and Meng, J.: Real-time and retrospective forcing in the North American Land Data Assimilation System (NLDAS) project, J. Geophys. Res., 108, 8842, doi:10.1029/2002JD003118, 2003. 5172

Dai, Y., Zeng, X., Dickinson, R. E., Baker, I., Bonan, G., Bosilovich, M., Denning, S., Dirmeyer, P., Houser, P., Niu, G., Oleson, K., Schlosser, A., and Yang, Z.-L.: The common land model (CLM), B. Am. Meteorol. Soc., 84, 1013–1023, doi:10.1175/BAMS-84-8-1013, 2003. 5170

Derber, J., Parrish, D., and Lord, S.: The new global operational analysis system at the National Meteorological Center, Weather Forecast., 6, 538–547, 1991. 5172

Ducharne, A., Koster, R., Suarez, M., Stieglitz, M., and Kumar, P.: A catchment-based approach to modeling land surface processes in a general circulation model. 2. Parameter estimation and model demonstration, J Geophys. Res., 105, 24823–24838, 2000. 5170

Ek, M. B., Mitchell, K. E., Yin, L., Rogers, P., Grunmann, P., Koren, V., Gayno, G., and Tarpley, J. D.: Implementation of Noah land-surface model advances in the NCEP operational mesoscale Eta model, J. Geophys. Res., 108, 8851, doi:10.1029/2002JD003296, 2003. 5170

Guo, Z., Dirmeyer, P. A., Gao, X., and Zhao, M.: Improving the quality of simulated soil moisture with a multi-model ensemble approach, Q. J. Roy. Meteor. Soc., 133, 731–747, 2007. 5169

Hansen, M., DeFries, R., Townshend, J., and Sohlberg, R.: Global land cover classification at 1 km spatial resolution using a classification tree approach, Int. J. Remote Sens., 21, 1331–1364, 2000. 5173

Huete, A. R., Didan, K., Shimabukuro, Y. E., Ratana, P., Saleska, S. R., Hutyra, L. R., Yang, W., Nemani, R. R., and Myneni, R.: Amazon rainforests green-up with sunlight in dry season, Geophys. Res. Lett., 33, L06405, doi:10.1029/2005GL025583, 2006. 5177

Ji, L. and Peters, A. J.: Assessing vegetation response to drought in the northern Great Plains using vegetation and drought indices, Remote Sensing of Environment, 87(1), 85-98, doi:10.1016/S0034-4257(03)00174-3, 2003. 5169

Ji, L. and Peters, A. J.: Lag and seasonality considerations in evaluating AVHRR NDVI response to precipitation, Photogramm. Eng. Rem. S., 71, 1053–1061, 2005. 5169

Kogan, F. N.: Droughts of the late 1980s in the United States as derived from NOAA polar orbiting satellite data, B. Am. Meteorol. Soc., 76, 655–668, 1995. 5169

Koster, R. D., Suarez, M. J., Ducharne, A., Stieglitz, M., and Kumar, P.: A catchment-based approach to modeling land surface processes in a general circulation model: 1. Model structure, J. Geophys. Res., 105, 24809–24822, doi:10.1029/2000JD900327, 2000. 5170, 5171

HESSD
9, 5167–5193, 2012

Drought monitoring utility

W. T. Crow et al.

Kumar, S. V., Peters-Lidard, C. D., Tian, Y., Houser, P. R., Geiger, J., Olden, S., Lighty, L., Eastman, J. L., Doty, B., Dirmeyer, P., Adams, J., Mitchell, K., Wood, E. F., and Sheffield, J.: Land Information System – An interoperable framework for high resolution land surface modeling, Environ. Modell. Softw., 21, 1402–1415, 2006. 5170

Mitchell, K.: The community Noah land-surface model: User Guide Public Release Version 2.7.1, available at: http://www.emc.ncep.noaa.gov/mmb/gcp/noahlsm/Noah_LSM_USERGUIDE_2.7.1.htm (last access: 13 April 2012), 2005. 5170

Mo, K. C., Long, L. N., Xia, Y., Yang, S. K., Schemm, J. E., and Ek, M. B.: Drought indices based on the Climate Forecast System Reanalysis and ensemble NLDAS, J. Hydrometeorol., 12, 185–210, 2010. 5168

Musyimi, Z.: Temporal Relationships Between Remotely-Sensed Soil Mositure and NDVI over Africa: Potential for Drought Early Warning, Master Thesis, University of Twenty, The Netherlands, 2010. 5169

Panu, U. S. and Sharma, T. C.: Challenge in drought research: Some perspectives and future directions, Hydrol. Sci. J., 47, S19–S30, 2002.

Peled, E., Dutra, E., Viterbo, P., and Angert, A.: Technical Note: Comparing and ranking soil drought indices performance over Europe, through remote-sensing of vegetation, Hydrol. Earth Syst. Sci., 14, 271–277, doi:10.5194/hess-14-271-2010, 2010. 5169, 5173

Peters, A. J., Walter-Shea, E. A., Ji, L., Vina, A., Hayes, M., and Svoboda, M. D.: Drought monitoring with NDVI-based Standardized Vegetation Index, Photogramme. Eng. Rem. S., 68, 71–75, 2002. 5169

Sheffield, J., Xia, Y., Luo, L., Wood, E. F., Ek, M., Mitchell, K. E., and the NLDAS Team: Drought monitoring with the North American Land Data Assimilation System (NLDAS): Current capabilities and future challenges, in: Remote Sensing and Drought, edited by: Wardlow, B., Anderson, M., and Verdin, J., CRC Press, 480 pp., 2012. 5168

Van Storch, H. and Zwiers, F. W.: Statistical Analysis in Climate Research, Cambridge Press, 484 pp., 2004. 5178

Wardlow, B., Anderson, M., and Verdin, J.: Remote Sensing and Drought, CRC Press, 480 pp., 2012. 5168, 5181

Xia, Y., Mitchell, K. E., Ek, M. B., Cosgrove, B., Sheffield, J., Luo, L., Alonge, C. J., Wei, H., Meng, J., Livneh, B., Duan, Q., and Lohmann, D.: Continental-scale water and energy flux analysis and validation for the North American Land Data Assimilation System project phase

2 (NLDAS-2): 1. Intercomparison and application of model products, J. Geophys. Res., 117, D03109, doi:10.1029/2011JD016048, 2012. 5172

Xie, P. and Arkin, P.: Global precipitation: A 17-year monthly analysis based on gauge observations, satellite estimates, and numerical model output, B. Am. Meteorol. Soc., 78, 2539–2558, 1997. 5172

HESSD
9, 5167–5193, 2012

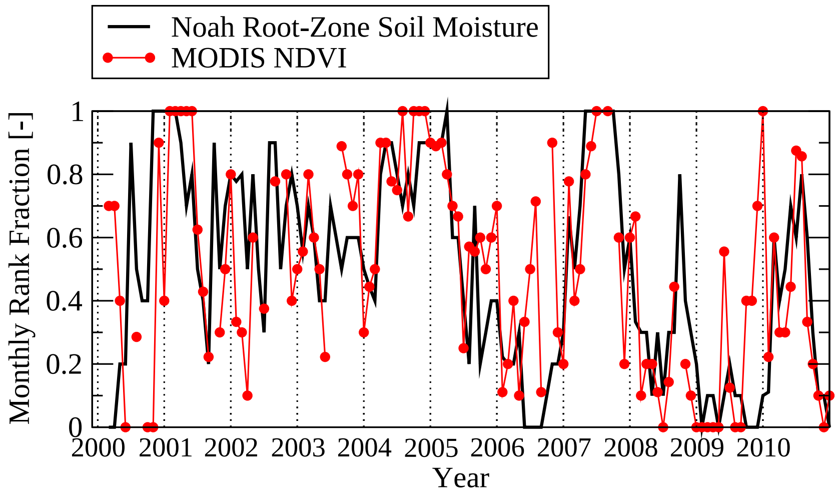

Fig. 1. Example monthly Rank($\overline{\text{NDVI}}$) and Rank($\bar{\theta}_{\text{Noah}}$) time series for a 0.25° pixel in the south-central United States.

HESSD

9, 5167–5193, 2012

Drought monitoring utility

W. T. Crow et al.

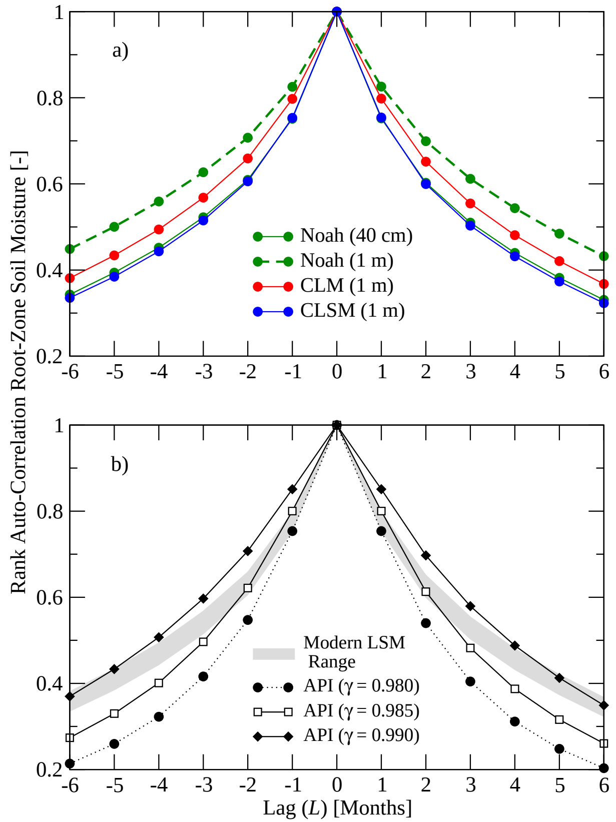

Fig. 2. Quasi-global land averages of $\rho(L)$ for **(a)** modern LSMs (i.e., Noah, CLM, and CLSM) and **(b)** various API cases. Noah results in **(a)** are shown for both a 40-cm and 1-m root-zone depth case. The "modern LSM" shading in **(b)** is defined as the absolute range of 40-cm Noah, 1-m CLM, and 1-m CLSM $\rho(L)$ results in **(a)**.

HESSD
9, 5167–5193, 2012

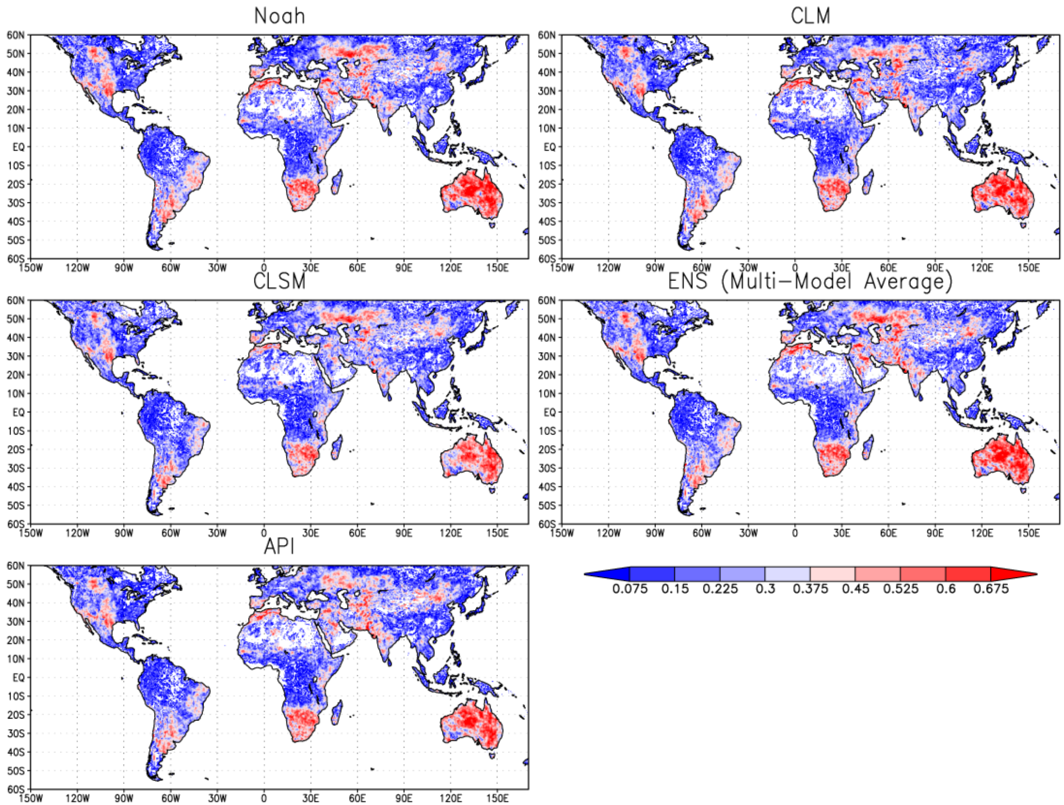

Fig. 3. Quasi-global map of 0.25° $R(-1)$ for the Noah, CLM, CLSM, ENS, and API cases.

HESSD
9, 5167–5193, 2012

Drought monitoring utility

W. T. Crow et al.

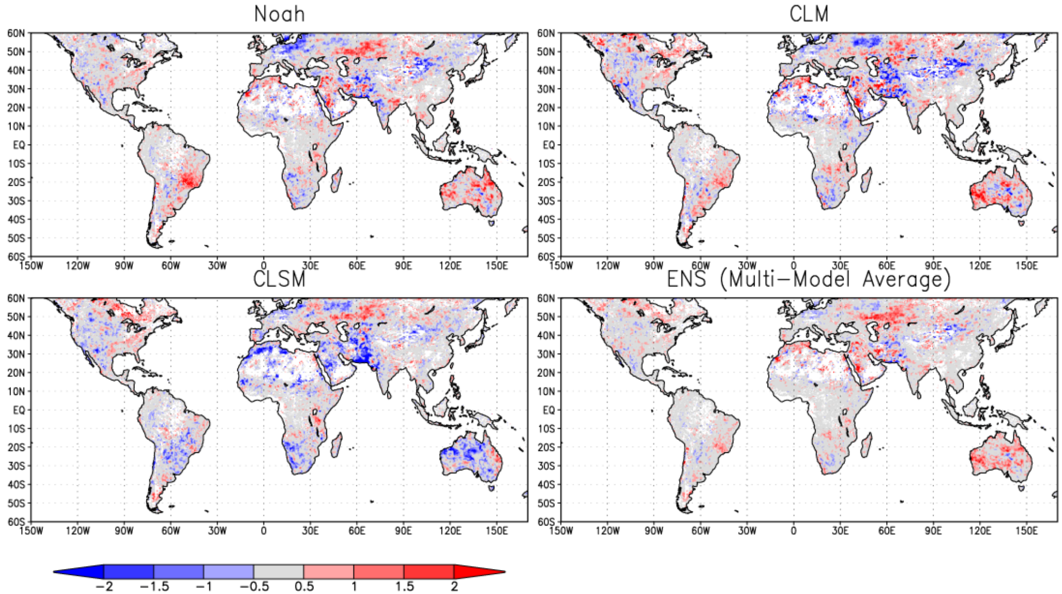

Fig. 4. Quasi-global map of 0.25° Z-scores for differences between Noah-based, CLM-based, CLSM-based, ENS-based $R(-1)$ and baseline API-based $R(-1)$.

HESSD
9, 5167–5193, 2012

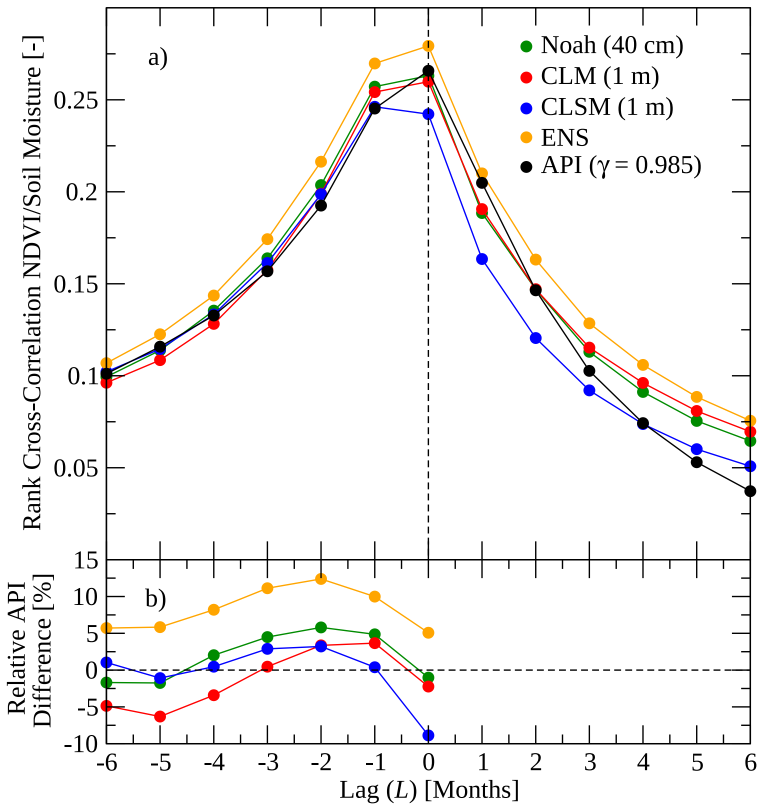

Fig. 5. Quasi-global land averages of: **(a)** $R(L)$ for Noah, CLM, CLSM, ENS, and API root-zone soil moisture predictions, and **(b)** percentage relative $R(L)$ difference for the modern LSMs (Noah, CLM, CLSM, and ENS) versus an API baseline (i.e., $100 * [R(L)_{\mathrm{LSM}} - R(L)_{\mathrm{API}}]/R(L)_{\mathrm{API}}$).

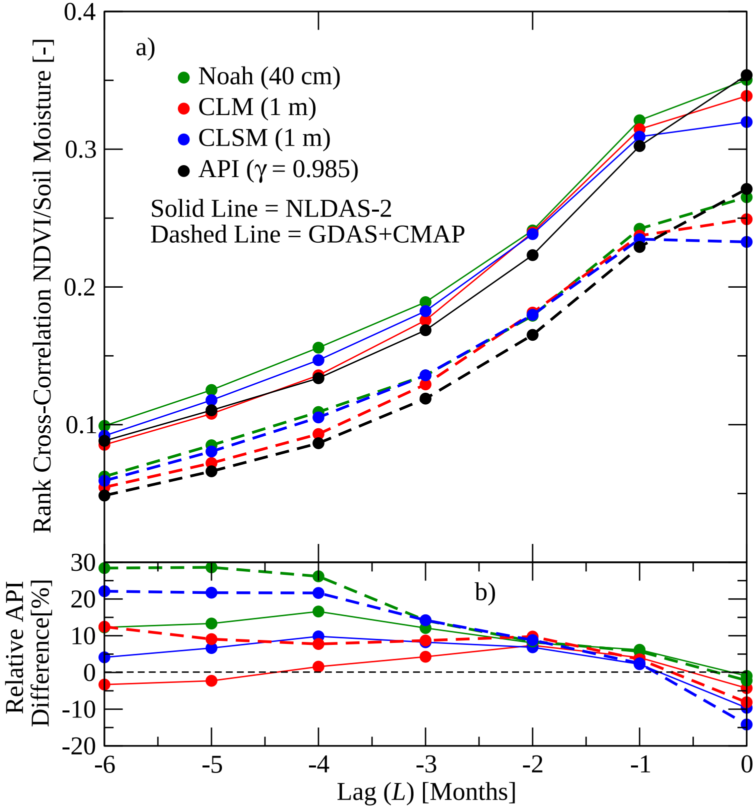

Fig. 6. CONUS land averages of: **(a)** $R(L)$ for Noah, CLM, CLSM, and API root-zone soil moisture predictions based on either the GDAS + CMAP or NLDAS-2 forcing data sets, and **(b)** percentage relative $R(L)$ percentage difference for the modern LSMs (Noah, CLM, and CLSM) versus an API baseline (i.e., $100 * [R(L)_{\text{LSM}} - R(L)_{\text{API}}]/R(L)_{\text{API}}$).

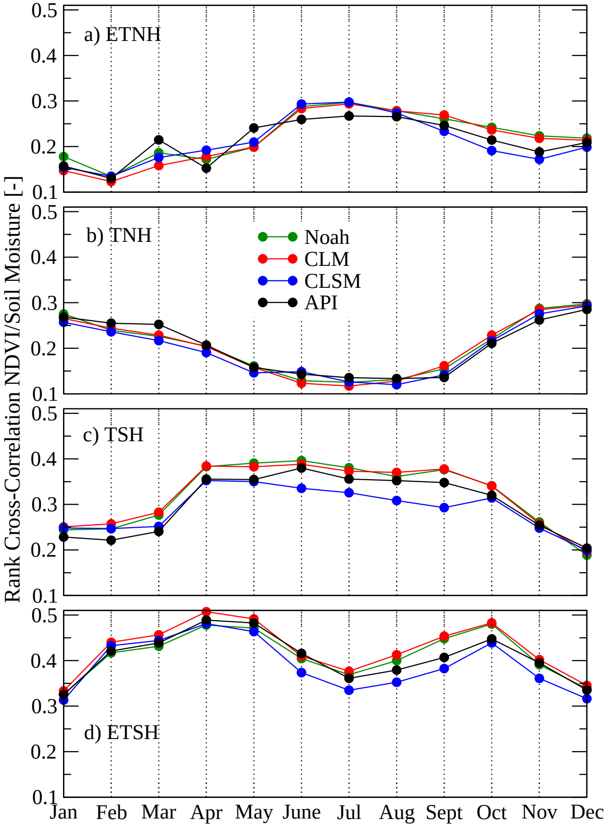

Fig. 7. Spatial averages of $R(-1)$ for Noah, CLM, CLSM, and API broken down by month-of-year for Rank($\bar{\theta}$) within the: **(a)** extra-tropical Northern Hemisphere (ETNH), **(b)** tropical Northern Hemisphere (TNH), **(c)** tropical Southern Hemisphere (TSH), and **(d)** extra-tropical Southern Hemisphere (ETSH).

HESSD
9, 5167–5193, 2012

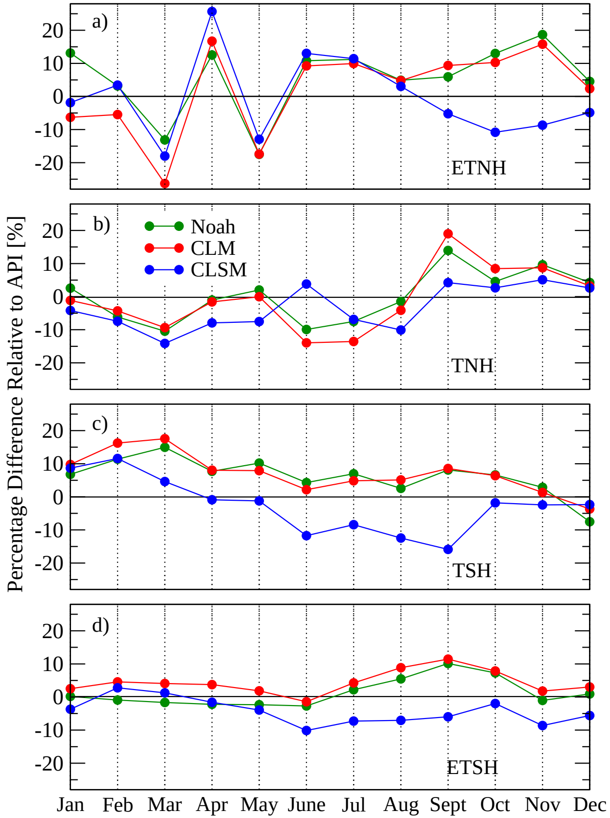

Fig. 8. Spatial averages of relative change in Noah, CLM, and CLSM $R(-1)$ results versus the API baseline (i.e., $100 * [R(-1)_{\mathrm{LSM}} - R(-1)_{\mathrm{API}}]/R(-1)_{\mathrm{API}}$) broken down by month-of-year for Rank($\bar{\theta}$) within the: **(a)** extra-tropical Northern Hemisphere (ETNH), **(b)** tropical Northern Hemisphere (TNH), **(c)** tropical Southern Hemisphere (TSH), and **(d)** extra-tropical Southern Hemisphere (ETSH).